AFRL-RY-WP-TP-2008-1154

GENERALIZED FREQUENCY-DOMAIN CORRELATOR FOR SOFTWARE GPS RECEIVER: PRELIMINARY TEST RESULTS AND ANALYSIS (PREPRINT)

Chun Yang, Mikel Miller, Thao Nguyen, and Dennis Akos

Sigtem Technology, Inc.

SEPTEMBER 2006

AIR FORCE RESEARCH LABORATORY
SENSORS DIRECTORATE
WRIGHT-PATTERSON AIR FORCE BASE, OH 45433-7320
AIR FORCE MATERIEL COMMAND
UNITED STATES AIR FORCE

REPORT DOCUMENTATION PAGE

Form Approved
OMB No. 0704-0188

1. REPORT DATE *(DD-MM-YY)*	2. REPORT TYPE	3. DATES COVERED *(From - To)*
September 2006	Conference Paper Preprint	08 April 2005 – 08 September 2006

4. TITLE AND SUBTITLE
GENERALIZED FREQUENCY-DOMAIN CORRELATOR FOR SOFTWARE GPS RECEIVER: PRELIMINARY TEST RESULTS AND ANALYSIS (PREPRINT)

5a. CONTRACT NUMBER
FA8650-05-C-1828

5b. GRANT NUMBER

5c. PROGRAM ELEMENT NUMBER
65502F

6. AUTHOR(S)
Chun Yang (Sigtem Technology, Inc.)
Mikel Miller and Thao Nguyen (AFRL/RYRN)
Dennis Akos (University of Colorado)

5d. PROJECT NUMBER
3005

5e. TASK NUMBER
13

5f. WORK UNIT NUMBER
300513CY

7. PERFORMING ORGANIZATION NAME(S) AND ADDRESS(ES)
Sigtem Technology, Inc.
1343 Parrott Drive
San Mateo, CA 94402-3630

Reference Systems Branch (AFRL/RYRN)
RF Sensor Technology Division
Air Force Research Laboratory, Sensors Directorate
Wright-Patterson Air Force Base, OH 45433-7320
Air Force Materiel Command, United States Air Force

University of Colorado

8. PERFORMING ORGANIZATION REPORT NUMBER

9. SPONSORING/MONITORING AGENCY NAME(S) AND ADDRESS(ES)
Air Force Research Laboratory
Sensors Directorate
Wright-Patterson Air Force Base, OH 45433-7320
Air Force Materiel Command
United States Air Force

10. SPONSORING/MONITORING AGENCY ACRONYM(S)
AFRL/RYRN

11. SPONSORING/MONITORING AGENCY REPORT NUMBER(S)
AFRL-RY-WP-TP-2008-1154

12. DISTRIBUTION/AVAILABILITY STATEMENT
Approved for public release; distribution unlimited.

13. SUPPLEMENTARY NOTES
Paper produced under contract FA8650-05-C-1828 for technical report AFRL-RY-WP-TR-2008-1137, SOFTWARE TOOLKIT FOR NONLINEAR FILTERS FOR GLOBAL POSITIONING SYSTEM (GPS) OPERATIONAL CONTROL SEGMENT (OCS) ESTIMATION AND OTHER APPLICATIONS.

Conference paper published in the Proceedings of the Institute of Navigation - 19th International Technical Meeting of the Satellite Division, ION GNSS 2006, Vol. 4 (held Sep 26-29 2006, Fort Worth, TX; Publisher: Institute of Navigation).

PAO Case Number: SN 06-0072; Clearance date: 15 Mar 2006. The U.S. Government is joint author of this work and has the right to use, modify, reproduce, release, perform, display, or disclose the work. Paper contains color.

14. ABSTRACT
The generalized frequency-domain correlator (GFDC) is introduced in this paper within the framework of a software GPS receiver which implements a frequency-domain baseband signal processor. The use of a GFDC can offer several advantages. First, as a generalization of the FFT-implemented correlation with a block repetitive processing capability, it enables fast acquisition through simultaneous code delay and Doppler frequency search. Second, it produces the delay-Doppler map of (generalized) complex correlations from which the joint code delay and carrier phase and frequency error discriminator can be implemented for grid tracking with the joint code and carrier loops, thus blurring the line between acquisition and tracking. Third, the same operation is applicable, without any other changes except for the replica code, to both the BPSK codes such as GPS C/A-code and the BOC modulations such as M-code.

Abstract concludes on reverse side →

15. SUBJECT TERMS

16. SECURITY CLASSIFICATION OF:			17. LIMITATION OF ABSTRACT:	18. NUMBER OF PAGES	19a. NAME OF RESPONSIBLE PERSON (Monitor)
a. REPORT	b. ABSTRACT	c. THIS PAGE			Thao Nguyen
Unclassified	Unclassified	Unclassified	SAR	22	19b. TELEPHONE NUMBER *(Include Area Code)* N/A

Standard Form 298 (Rev. 8-98)
Prescribed by ANSI Std. Z39-18

14. ABSTRACT (concluded)

Fourth, it can switch seamlessly among different types of correlation/matching operations with a wide peak base for acquisition and a narrow peak base for tracking. Fifth, the generalized correlation has a sharp peak with a reduced base width, thus making its timing estimation more accurate and less sensitive to multipath.

In this paper, the generalized frequency-domain correlator (GFDC) is formulated and different implementation schemes for spectrum filtering are presented. The experimental data (a set GPS data recorded on a large aircraft) are used to demonstrate the ability of the GFDC to uncover closely-spaced multipath signals more easily than the conventional correlators. The practical issue of limited signal bandwidth and its effects on both the conventional correlators and the GFDC are analyzed via computer simulation.

Generalized Frequency-Domain Correlator for Software GPS Receiver: Preliminary Test Results and Analysis

Chun Yang, *Sigtem Technology, Inc.*
Mikel Miller, Thao Nguyen, *Air Force Research Lab/RYRN*
Dennis Akos, *University of Colorado*

BIOGRAPHIES

Dr. Chun Yang received his title of Docteur en Science from the Université de Paris (No. XI, Orsay), France, in 1989. After two years of post-doctoral research at the University of Connecticut, he moved on with his industrial R&D career. Since 1993, he has been with Sigtem Technology, Inc. and has been working on numerous GPS, integrated inertial, and adaptive array related projects.

Dr. Mike Miller is the Technical Advisor for the Reference Systems Branch, Sensors Directorate, Air Force Research Laboratory, WPAFB, OH. He received his Ph.D. in Electrical Engineering from the Air Force Institute of Technology (AFIT), WPAFB, Ohio, in 1998. Since 1986, he has focused on navigation system R&D related to GPS, GPS/INS integrations, alternative navigation techniques including bio-inspired navigation and signals of opportunity based navigation, autonomous vehicle navigation and control, and multi-sensor fusion. He is currently responsible for both in-house and contracted R&D projects advancing navigation technology. He is also an Adjunct Professor of EE at AFIT and Miami University of Ohio. Dr Miller is a member of the ION, RIN, IEEE, and AIAA.

Thao Q. Nguyen is a Ph.D. candidate in the Electrical and Computer Engineering Department at the Air Force Institute of Technology (AFIT), Wright-Patterson AFB, Ohio. He also works as an Electronics Engineer at the Reference Systems Branch, Sensors Directorate, Air Force Research Laboratory, WPAFB OH. Mr. Nguyen has been involved with navigation-related research, development, and test since 2002 and his current areas of interest include high anti-jamming technologies for GPS receivers, GPS/INS integration, multi-sensor fusion, and personal navigation using signal of opportunity (SoOP).

Dennis M. Akos is currently an Assistant Professor with the Aerospace Engineering Science Department at University of Colorado at Boulder. He has also since served as a faculty member with Luleå Technical University, Sweden and a Research Associate with the GPS Laboratory at Stanford University. He obtained the Ph.D. degree in Electrical Engineering at Ohio University within the Avionics Engineering Center.

ABSTRACT

The generalized frequency-domain correlator (GFDC) is introduced in this paper within the framework of a software GPS receiver which implements a frequency-domain baseband signal processor. The use of a GFDC can offer several advantages. First, as a generalization of the FFT-implemented correlation with a block repetitive processing capability, it enables fast acquisition through simultaneous code delay and Doppler frequency search. Second, it produces the delay-Doppler map of (generalized) complex correlations from which the joint code delay and carrier phase and frequency error discriminator can be implemented for grid tracking with the joint code and carrier loops, thus blurring the line between acquisition and tracking. Third, the same operation is applicable, without any other changes except for the replica code, to both the BPSK codes such as GPS C/A-code and the BOC modulations such as M-code. Fourth, it can switch seamlessly among different types of correlation/matching operations with a wide peak base for acquisition and a narrow peak base for tracking. Fifth, the generalized correlation has a sharp peak with a reduced base width, thus makes its

timing estimation more accurate and less sensitive to multipath.

In this paper, the generalized frequency-domain correlator (GFDC) is formulated and different implementation schemes for spectrum filtering are presented. The experimental data (a set GPS data recorded on a large aircraft) are used to demonstrate the ability of the GFDC to uncover closely-spaced multipath signals more easily than the conventional correlators. The practical issue of limited signal bandwidth and its effects on both the conventional correlators and the GFDC are analyzed via simulation.

INTRODUCTION

At the heart of a GPS receiver is the baseband signal processor made of correlators (or matched filters) embedded in code and carrier tracking loops. Successful correlating of the incoming signal with a reference code enables a receiver to identify from which GPS satellite the acquired signal originates, to provide the processing gain necessary for code lag and carrier phase and frequency estimation, and to accumulate samples for navigation data bit sync and demodulation. These and other pieces of information extracted from the signal lead to the GPS observables and satellite ephemeredes for ultimate finding of a position, navigation, and time (PNT) solution [Parkinson and Spilker, 1996; Kaplan, 1996; Tsui, 2000; Misra and Enge, 2001].

In conventional GPS receivers, since the incoming GPS signal and the local replica are typically quantized with a small number of bits, the correlators can be implemented using extremely simple logic circuits such as XOR followed by equally simple accumulators (integrate-and-dump). Hundreds and even thousands of such correlators have been integrated in a single small-size low-power IC chip. However, the time-domain implementation of a correlation function as in most conventional GPS receivers runs into certain inherent properties of correlation that may become limitations for some high performance applications.

For a maximum-length pseudo-random number (PRN) code, its correlation function is ideally an equilateral triangle with its base width being $\pm T_c$ where $T_c = 1/f_c$ is the chip duration and f_c is the chipping rate. See Figure 1 for illustration. To ensure an acceptable level of signal to noise ratio (SNR), the tolerable code delay error is limited to $\Delta t = T_c/2$ (this produces the worst signal loss of 2.5 dB) and the frequency error is limited to $\Delta f \le 1/2T_i$ where T_i is the despreading integration time interval (this introduces another loss of 0.9 dB). Without knowing the signal parameters as in a cold start, a GPS receiver has to conduct an initial search sequentially in the time and frequency uncertainty zone to reduce the signal parameter errors prior to closing the tracking loops.

The shape of a correlation function is code-dependent, thus requiring a special correlator structure for each type of codes. For examples, the binary phase shift keying (BPSK) type of codes such as GPS C/A-code and P-code has its correlation function of a triangle shape. In contrast, the newly introduced binary offset carrier (BOC) modulation such as M-code and L1C-code (under development) as well as the European Galileo codes has numerous nulls and sidelobes in its correlation function. Although the mainlobe is narrow, the sidelobes are not substantially smaller. Without special hardware and software, a receiver runs the risk of being trapped in nulls (i.e., missing detection) or locking onto a sidelobe (i.e., biased measurements) [Fine and Wilson, 1999; Betz, 2001].

It is well-known that timing measurements derived from a correlation function are subject to multipath errors. When the correlation function is sampled by hardware or software correlators with a spacing of d, any multipath signal with a delay $\tau < (1+d)T_c$ can superimpose its own correlation onto the direct signal's. Since the composite correlation function is distorted more on the late side than on the early side, the symmetry is distorted with the zero crossing of the delay error discriminator (the early-minus-late correlation type) moved away from the true timing. This multipath-induced timing error is translated into the GPS ranging errors. In general, the smaller the correlator spacing and chip duration, the smaller are the multipath code errors. This explains why a P(Y)-code has better multipath performance than a C/A-code and why a receiver with narrow correlators can reject multipath better. Again, this is also code-dependent.

In this paper, we present some preliminary test results of the newly introduced generalized frequency-domain correlator (GFDC) with recoded GPS data [Miller, Nguyen, and Yang, 2006]. It is a natural yet proliferous extension of the Fast Fourier Transform (FFT)-implemented correlation by incorporating direct manipulation of the incoming signal, replica, and correlation spectra. With the repetitive processing capability for code delay and Doppler frequency search [Yang, Miller, and Nguyen, 2006], it produces a delay-Doppler map of the complex correlation that blurs the line between acquisition and tracking [Yang, 2001a].

With different spectral processing, the GFDC allows for the implementation of a channel impulse response

[Yang and Miller, 2005] or a symmetric phase-only matched filter (SPOMF) [Miller, Nguyen, and Yang, 2006] or both in a sequential manner. As one of the main advantages, the GFDC is uni-modal without the presence of multipath and does not depend on the underlying code structure. As a result, the same receiver architecture can be used for both BPSK- and BOC-types of codes.

It further offers better multipath performance. Ideally, the GFDC (e.g., the satellite signal channel impulse response or the symmetric phase-only matched filter) produces a Dirac delta function. It thus has an infinite time resolution capability and is immune to multipath. In practice, however, both the GPS signals and receivers are band-limited to a half of the sampling rate f_s. The resulting peak is of the shape of a *sinc* function with its first nulls at $\pm T_s$, where $T_s = 1/f_s$ is the sampling interval. Even so, the peak still has its base width much narrower than that of a correlation function (i.e., $T_s < T_c$). As such, it is less sensitive to multipath than conventional receivers [Yang and Porter, 2005]. In addition, it may reveal the presence of close-in multipath signals that are otherwise difficult to discern as they are lumped into an enlarged conventional correlation peak. In reality, however, the peak width T_{eff} is determined by the effective bandwidth f_{eff} of the GPS signal and the transmitter-receiver combined (i.e., $T_{eff} = 1/f_{eff}$). Figure 1 illustrates the relationships where except for the impulse Dirac delta function and the ideal triangular correlation function, other functions exhibit more or less the *sinc*-like shape.

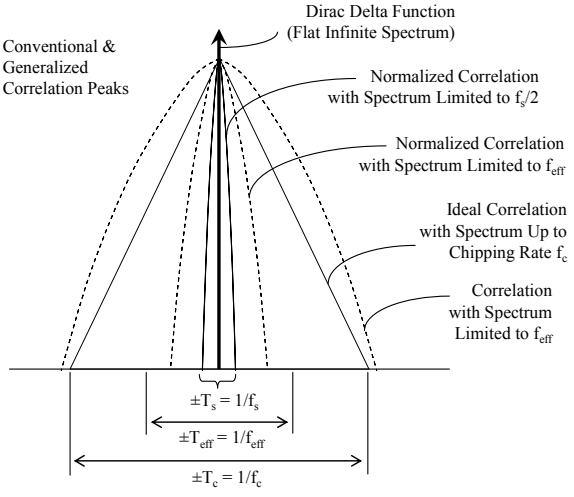

Figure 1 – Width and Shape of Generalized Correlation Peaks

Moreover, a GFDC can benefit from such properties of a frequency-domain GPS receiver as fast acquisition with simultaneous search in time and frequency, narrowband interference suppression, joint code and carrier tracking with a joint error discriminator [Yang, 2001a, 2003, 2004], and full-band multi-code processing [Yang, 2005].

The rest of paper is organized as follows. The concept and formulation of the generalized frequency-domain correlator (GFDC) are first introduced. The experimental data that are used in this paper to test the GFDC are described next. The processing results are then presented to demonstrate the ability of the GFDC to uncover closely-spaced multipath signals more easily than the conventional correlators. Finally, the practical issue of limited bandwidth and its effects on both conventional correlators and GFDC are analyzed and compared via simulation.

GENERALIZED FREQUENCY-DOMAIN CORRELATOR (GFDC)

The generalized frequency-domain correlator (GFDC) is introduced in this paper within the framework of a software GPS receiver which implements a frequency-domain baseband processor as shown in Figure 2. The use of a GFDC has several advantages. First, as a generalization of the FFT-implemented correlation with a block repetitive processing capability, it enables fast acquisition through simultaneous code delay and Doppler frequency search. Second, it produces the delay-Doppler map of (generalized) complex correlations from which the joint code delay and carrier phase and frequency error discriminator can be implemented for grid tracking with the joint code and carrier loops, thus blurring the line between acquisition and tracking. Third, the same operation is applicable, without any other changes except for the replica code, to both the BPSK codes such as GPS C/A-code and the BOC modulations such as M-code. Fourth, it can switch seamlessly among different types of correlation/matching operations with a wide base for acquisition and a narrow base for tracking. Fifth, it has a sharp peak in the generalized correlation with the reduced width, which makes its timing estimation more accurate and less sensitive to multipath.

This GFDC differs from the generalized cross correlator (GCC) that has been used for radar and sonar signal processing for delay estimation [Knapp and Carter, 1976; Hassab and Boucher, 1979]. The GCC is closely related to the coherence, a complex quantity that is the cross-power spectral density between two random processes divided by the

product of their auto power spectral densities. The design goal of the GCC is to produce the highest SNR correlation peaks in the presence of noise. The optimum filter is designed with the spectral characteristics of the noise assumed to be known. As pointed out in [Wernet, 2005], some of these filters alter the phase of the input functions, which could bias the final output.

As shown in Figure 2, the GFDC accepts the incoming signal s(t) and the code replica r(t) and produces the generalized correlation function c(t) between the two. This is the same input-output behavior as other correlators. However, what makes it different is the spectrum filtering, namely, U(f), V(f), and W(f) applied along the signal processing chain, as well as the feedback paths inserted in the frequency domain. Clearly, when there is no spectrum manipulation and feedback, it becomes a simple straight FFT-implemented correlation. Various spectrum filtering schemes can be applied that makes the GFDC design versatile, which are described below.

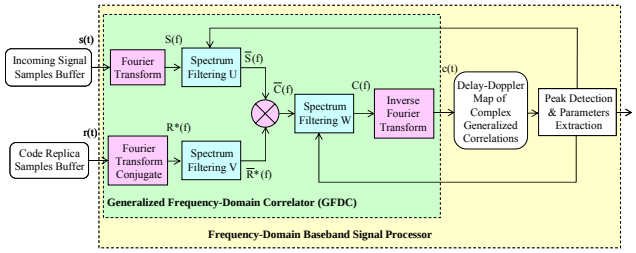

Figure 2 – Generalized Frequency-Domain Correlator (GFDC) Architecture

Examples of Spectrum Windowing/Filtering

GPS baseband signal processing is block-oriented and a block (or a segment) of incoming signal samples are operated upon during despreading integration or correlation. For a frequency-domain baseband processor, the "overlap and discard" algorithm is typically used to implement the correlation over T_i [Yang, 2001b]. It calls for $2T_i$ of incoming signal samples so as to contain at least a code sequence free of navigation data bit sign reversal whereas the replica samples of T_i are appended with T_i zeros to have the same length. For the purpose of this paper, it suffices to denote the number of samples per block by N. In reference to Figure 2, introduce the following array (vector) notations for the input and output data per block and their relationships:

$$\underline{s} = [s(t),\ t = 0, 1, \ldots, N\text{-}1]^T \quad (1a)$$
$$\underline{S} = [S(f),\ f = 0, 1, \ldots, N\text{-}1]^T \quad (1b)$$
$$S(f) = FT\{s(t)\} = \sum_{t=0}^{N-1} s(t)\exp\{\frac{-j2\pi ft}{N}\} \quad (1c)$$
$$s(t) = IFT\{S(f)\} = \frac{1}{N}\sum_{f=0}^{N-1} S(f)\exp\{\frac{j2\pi ft}{N}\} \quad (1d)$$

where the superscript T stands for vector or matrix transpose, FT{·} and IFT{·} represent the Fourier transformation and inverse Fourier transformation, respectively, and the time index t is relative to the first sample of the block, which is typically time-tagged in terms of the receiver clock ticks.

$$\underline{r} = [r(t),\ t = 0, 1, \ldots, N\text{-}1]^T \quad (2a)$$
$$\underline{R} = [R(f),\ f = 0, 1, \ldots, N\text{-}1]^T \quad (2b)$$
$$\underline{R} = FT\{\underline{r}\} \quad (2c)$$
$$\underline{r} = FT\{\underline{R}\} \quad (2d)$$

where FT{·} and IFT{·} are also used to relate the Fourier transform and inverse Fourier transform of the entire data blocks, respectively.

$$\underline{c} = [c(t),\ t = 0, 1, \ldots, N\text{-}1]^T \quad (3a)$$
$$\underline{C} = [C(f),\ f = 0, 1, \ldots, N\text{-}1]^T \quad (3b)$$
$$\underline{C} = FT\{\underline{c}\} \quad (3c)$$
$$\underline{c} = FT\{\underline{C}\} \quad (3d)$$

The (generalized) correlation spectrum is related to the filtered input signal and replica spectra, on a frequency bin to bin basis and in vector formats, respectively, by:

$$\overline{C}(f) = \overline{S}(f)\overline{C}^*(f),\ f = 0, \ldots, N\text{-}1 \quad (4a)$$
$$\underline{\overline{C}} = diag\{\underline{\overline{S}}\}\underline{\overline{C}}^* = [\overline{S}(f)\overline{C}^*(f),\ f = 0,1,\ldots,N-1]^T \quad (4b)$$

where the superscript * stands for complex conjugate and *diag(*$\underline{v}$*)* stands for a diagonal matrix with its diagonal elements specified by the vector $\underline{v}$.

There are two types of spectrum filtering involved in the generalized frequency-domain correlator. The first is an operation that is applied to individual frequency bins. This can occur to the incoming signal spectrum, the replica spectrum, and the correlation spectrum as well. Due to the linear nature of the operation in Eq. (4), these per bin filtering operations can be either lumped together at one place (which has computational advantages) or separated (which makes the filtering easier to understand). The second type of operations involves the entire spectrum and is therefore sensitive to the order in which it is placed along the processing chain.

In the following, we introduce some filters and additional filters can be found in [Miller, Nguyen, and Yang, 2006].

Spectrum Excision of Narrowband Interference. Being spread spectrum, the GPS signal is below the thermal noise. Any spikes in the signal spectrum are attributed to interference and as such, the spectrum

values at those frequency bins can be removed and replaced with zeros. This requires continuous monitoring of the spectrum and power-detection against a pre-defined threshold [Yang, Vasquez, and Chafee, 1999]. The operation of excision can be viewed as passing the signal through a notch filter in the time domain or equivalently as multiplying the spectrum with zero at those frequency bins of interference. To remove an interference component at the k^{th} frequency bin, the following operation is applied:

$$\underline{\bar{S}} = U_1^k \underline{S} \quad (5a)$$

$$U_1^k = diag(\begin{bmatrix} \underline{1}_{k-1}^T & 0 & \underline{1}_{N-k}^T \end{bmatrix}) \quad (5b)$$

where $\underline{1}_n$ is a vector of n ones (1's). The subscript of U_i is used in this (i = 1) and the following notations (i = 2, 3, 4) to indicate the different type of windowing/filtering. The operation can be repeated for all frequency bins of interest. It is implied that the same operation is applied to both corresponding positive and negative frequency bins at the same time if the signal is real-valued. Two popular ways to apply this spectral filtering are (1) zone-zeroing and (2) individual excision. The net effect of n operations from k_1 to k_n is given by:

$$U_1 = U_1^{k_n} \cdots U_1^{k_1} \quad (6)$$

Spectrum Segmentation of Multiple Codes. When it is desired to process each GPS signal band (L1, L2, or L5) while the full spectrum is available from a wideband receiver, the spectrum for individual codes can be extracted from the full band spectrum separately [Yang, 2005]. The operation can be viewed as passing the signal through a bandpass filter in the time domain or equivalently as selecting the spectrum at those frequency bins of interest. Both are linear operations. Assume we want to segment the spectrum at frequency bins from i to j. The following matrix multiplication implements an ideal bandpass filtering:

$$\underline{\bar{S}} = U_2^{i,j} \underline{S} \quad (7a)$$

$$U_2^{i,j} = diag([\underline{0}_{i-1}^T, \underline{1}_{j-i+1}^T, \underline{0}_{N-j}^T]) \quad (7b)$$

where $\underline{0}_n$ is a vector of n zeros (0's).

Spectrum Translation for Residual Doppler Removal with Feedback. The residual Doppler in the incoming signal appears as a multiplicative sine or cosine term to the code sequence, thus introducing a phase change from sample to sample. It is typically removed by multiplying the incoming signal with a carrier replica in the form of complex exponential at the desired Doppler frequency. This time-domain phase rotation is equivalent to spectrum translation in the frequency domain [Yang, Vasquez, and Chafee, 1999]. To remove a residual Doppler of ±dΔf Hz where Δf is the frequency resolution (i.e., the width of each frequency bin), the spectrum is down (up)-translated by d bins.

$$\underline{\bar{S}} = U_3^d \underline{S} \quad (8a)$$

$$U_3^{d=0} = I \quad (8b)$$

$$U_3^{d\neq 0} = \begin{bmatrix} 0 & \underline{0}_{d-2}^T & 1 & \underline{0}_{N-d}^T \\ \vdots & \vdots & \vdots & \vdots \\ 0 & \underline{0}_{N-3}^T & 0 & 1 \\ 1 & 0 & \underline{0}_{N-3}^T & 0 \\ \vdots & \vdots & \vdots & \vdots \\ \underline{0}_{N-2}^T & 1 & 0 & \underline{0}_{N-d}^T \end{bmatrix} \quad (8c)$$

where the first non-zero element of the first row is at the d^{th} column when d > 0 and at the $(N+d)^{th}$ column when d < 0. Since the matrix multiplication in Eq. (8a) is equivalent to index permutation, practical implementation resorts to circular shifted indexing of the array rather than actual matrix multiplication.

Without knowing the residual Doppler frequency, the initial search will select a large value for d so as to cover the frequency uncertainty interval. However, in the tracking mode, the estimated Doppler and its uncertainty will reduce it to a small interval from d_0-1 to d_0+1 for instance where d_0 is the closest bin to the estimated frequency. The top feedback line shown in Figure 2 indicates the need to repeat the operation for each and every frequency bin, producing a delay-Doppler map of generalized complex correlations.

Spectrum Windowing/Filtering. The spectrum windowing/filtering can be expressed as:

$$U_4 = diag\{[U(f), f = 0,\ldots,N-1]\} \quad (9a)$$

$$U(f) = \frac{U_0}{|S(f)|^\alpha}, \ \alpha = 0, \tfrac{1}{2}, 1, 2 \quad (9b)$$

$$U(f) = \frac{U_0}{|R(f)|^\beta}, \ \beta = \tfrac{1}{2}, 1 \quad (9c)$$

where U_0 is a real constant and α and β are design parameters with typical values given.

With Eq. (9b), the incoming signal spectrum is normalized by the incoming signal spectrum magnitude exponentially raised to the order α whereas with Eq. (9c), it is normalized by the replica spectrum magnitude exponentially raised to the order β. Without noise and other unknown effects on the incoming signal, the two operations would be exactly the same.

Since the GPS signal spectrum falls off with increasing frequency, the inverse magnitude windowing function of Eq. (9b) or (9c) acts as a high-pass filter, which tends to emphasize the edge

information without affecting the phase information. Since high frequency information decorrelates quickly, it helps to produce a very sharp correlation peak. This operation equalizes the magnitude spectrum, thus keeping the phase-only information.

The above spectrum filtering techniques can also be applied to the replica spectrum, although it may not serve the same purposes and not all of them are applicable at the same time. For example, instead of down-converting the incoming signal from IF to baseband, it is possible to up-convert the code replica from baseband to IF so as to catch up with the incoming signal by accounting for the unknown Doppler shift. This operation is similar to the spectrum translation described above.

Similarly, a windowing function can be applied to the (generalized) correlation spectrum. This can shape the correlation function for the inverse Fourier transform to be taken. Design goals include (1) reducing the sidelobe level, (2) maximizing the correlation peak, and (3) narrowing the mainlobe. However, these goals typically are not compatible to each other. Reducing the sidelobe level comes at a price of enlarging the mainlobe. Another useful operation is to evaluate the correlation function at a desired code lag. In the acquisition mode, since the code phase is unknown, a large interval of code phase (timing) uncertainty is searched. However, once in the tracking mode, the estimated code phase and its uncertainty can be used to place code lags where the correlation function is evaluated [Yang, 2003]. The bottom feedback line shown in Figure 2 indicates the number and location of the code lags to be evaluated.

When the spectrum windowing functions U_4 and V_4 are considered, the equivalence between the separate filtering operations and the joint filtering operation can be established as follows. Referring to Figure 2 again, we have:

$$\begin{aligned}\underline{C} &= W\underline{\overline{C}} = W diag\{\underline{\overline{S}}\}\underline{\overline{R}}^* = W diag\{U_4 S\}V_4\underline{R}^* \\ &= WU_4V_4 diag\{\underline{S}\}\underline{R}^* = \overline{W}\,\underline{\widetilde{C}}\end{aligned} \tag{10}$$

where $\overline{W} = WU_4V_4$ and $\underline{\widetilde{C}} = \text{diag}\{\underline{S}\}\underline{R}^*$.

Since U_4 is a diagonal matrix, it is easy to show that $\text{diag}\{U_4\underline{S}\} = U_4\text{diag}\{\underline{S}\}$, which is used to derive the last equality in Eq. (10).

Schemes for GFDC Implementation

Given the possible ways to filter the incoming signal, replica, and correlation spectra jointly or separately, we consider five special cases for the GFDC implementation.

Correlation Function. In the first case where U(f) = V(f) = W(f) = 1 for f = 0, 1, …, N-1, the generalized correlation spectrum becomes:

$$C(f) = S(f)R^*(f) \tag{11a}$$
$$c(t) = \text{IFT}\{C(f)\} \tag{11b}$$

Eq. (11a) is the conventional correlation spectrum and Eq. (11b) is the FFT-implemented cross-correlation.

Signal Channel Transfer Function/Impulse Response. In the second case where U(f) = V(f) = 1/|R(f)| and W(f) = 1 for f = 0, 1, …, N-1, the generalized correlation spectrum becomes:

$$C(f) = \frac{S(f)R^*(f)}{|R(f)|^2} = \frac{S(f)}{R(f)} \tag{12a}$$
$$h(t) = \text{IFT}\{C(f)\} \tag{12b}$$

Eq. (12a) is also called the GPS signal channel transfer function and Eq. (12b) is the corresponding impulse response.

Although V(f) = 1/|R(f)| effectively extracts the phase-only information from the replica R(f), U(f) may fail to do so because S(f) generally differs from R(f) due to residual Doppler and noise. By consequence, some spectral spikes show up near multiples of chipping rate where noise dominates. To suppress such noise amplification effects, spectral filtering such as zone-zeroing and individual excision can be applied [Yang and Porter, 2005; Yang and Miller, 2005].

Phase-Only Matched Filter (POMF). In the third case where U(f) = 1, V(f) = 1/|R(f)|, and W(f) = 1 (or equivalently, U(f) = V(f) = $|R(f)|^{-½}$ and W(f) = 1) for f = 0, 1, …, N-1, the generalized correlation spectrum becomes:

$$C(f) = \frac{S(f)R^*(f)}{|R(f)|} \tag{13}$$

In this operation, the incoming signal is correlated with a phase-only version of the replica, hence the name "phase-only." Since the incoming signal may differ from the replica greatly in magnitude, the POMF may perform poorly in some cases.

Symmetric Phase-Only Matched Filter (SPOMF). In this case where U(f) = 1/|S(f)|, V(f) = 1/|R(f)|, and W(f) = 1 for f = 0, 1, …, N-1, the generalized correlation spectrum becomes:

$$C(f) = \frac{S(f)}{|S(f)|}\left[\frac{R(f)}{|S(f)|}\right]^* = \frac{S(f)R^*(f)}{|S(f)||R(f)|} \tag{14}$$

In Eq. (14), S(f)/|S(f)| removes the magnitude information from the incoming signal spectrum and retains only the phase information. Similarly,

R(f)/|R(f)| removes the magnitude information from the code replica spectrum and retains only the phase information. The equalization is applied to both the incoming signal and replica, hence the name "symmetric." Since both the incoming signal and replica amplitude contents are involved in weighting, the spectral filtering is therefore "balanced."

Eq. (14) can also be viewed as the normalization of the correlation spectrum $S(f)R^*(f)$ by its magnitude spectrum $|S(f)R^*(f)|$.

Square-Root Normalized Correlation. Another variation is to normalize the incoming signal and the replica spectra with the square root of their respective magnitude spectrum, that is, $U(f) = |S(f)|^{-½}$, $V(f) = |R(f)|^{-½}$, and $W(f) = 1$ for $f = 0, 1, \ldots, N-1$, the generalized correlation spectrum becomes:

$$C(f) = \frac{S(f)R^*(f)}{\sqrt{|S(f)||R(f)|}} \qquad (15)$$

The generalized correlation as defined above involves, in one form or another, the division between the spectra of the incoming signal and its replica, which can be viewed as the output and input of a linear system, respectively. At a first glance, there may be a stability issue if the denominator contains a minimum-phase filter (as is mostly the case) which cannot be perfectly canceled in the spectrum normalization (division) because the numerator and denominator represent different filtering. However, with proper handling of those spectral lines with zero or small values, the operation is stable. This can be understood as the problem of identifying a well-behaved linear stable system (i.e., the generalized correlation). No matter what an excitation (the denominator, provided it is rich enough) is applied to the system, the system model can be recovered from the response (the numerator).

Ideally, a flat infinite spectrum produces a Dirac delta function in the time domain. By eliminating the shape information from the two input spectra, the phase only filtering (attenuating the magnitude information and accentuating the phase information in the frequency domain) can sharpen the correlation peak in the time domain.

The importance of phase in signals has been recognized for many applications in which a signal can be recovered completely or in part from knowledge of its phase alone. In a number of contexts [Oppenheim and Lim, 1981], the Fourier transform's phase data contains more of the "important" information than the Fourier transform's magnitude data. In a sense, the phase reflects the location of "events" more than the magnitude whereas the magnitude contains information more relevant to the size and shape of an object. The time shift property is an example: a translation in position (time or space) of a signal has no effect on the Fourier transform magnitude but only affects the phase by adding a linear phase term.

Conditions are given in [Oppenheim and Lim, 1981] under which the spectral magnitude is uniquely specified to within a scaling factor by its phase function. For example, the log magnitude of the Fourier transform is the Hilbert transform of the phase of a signal with all poles and zeros lying in the left half (the minimum-phase condition) or in the right half of the s-plane (the maximum-phase condition).

Since the autocorrelation function of phase-only signals is always an impulse, this feature has been used in designing methods for image registration and recognition [Chen, Defrise, and Deconinck, 1994] and digital image velocimetry [Wernet, 2005].

PRELIMINARY TEST RESULTS AND ANALYSIS

After describing the test data used in our study, we will present the processing results with the GFDC, focusing on its ability to uncover multipath as compared to conventional correlation.

Description of Test Data with Multipath

The recoded data used for this study were described in detail in [Akos et al., 2004]. It was collected on the back of a large aircraft when it was stationary near a hugger and during the flight with bank and turn maneuvers. The presence of multipath in the data was confirmed by analysis and other processing methods as described in the paper.

The data were collected with a special RF front-end designed specifically for the experiment. Due to the fact that any airframe multipath is expected to be short-delay multipath arriving soon after the direct signal, the operational bandwidth of the front-end was increased to 6 MHz (double sided) in order to better distinguish this type of multipath. The increase in bandwidth was a compromise between correlation peak sharpness and the required storage and processing rates. The L1 signal at 1575.42 MHz is beat with a LO at 1527.68 MHz. The resulting IF frequency is at 47.74 MHz. The final BPF 3 dB bandwidth is 6 MHz, which is larger than a typical choice of 2 MHz.

The sampling frequency was selected quite specifically at 17.357737 MHz (adjusted away from the initial frequency specification of 17.36 MHz) so that problematic harmonic components fell directly

between two adjacent VHF channels, thus eliminating the undesired interference problem. The signal was quantized in 4 bits.

Figure 3 shows the power spectrum density in dB. It was calculated using 8192-point FFT averaged over the first 10^{20} data points (using the MATLAB function *psd*). The mean value was removed from the data prior to the spectrum estimation. Otherwise, there would be a strong component at DC. The mean value is -0.6294 over 10^{20} data points, a significant bias due to the particular ADC/sampling scheme used. This DC component can be seen from the time-domain waveform where the negative full scale (-8) was more frequent than the positive full scale (7). The sample histogram is shown in Figure 4, which exhibits a fair resemblance to a Gaussian shape.

Uncovering of Multipath with GFDC vs. Conventional Correlation

One purpose of this study is to determine if the GFDC can indeed more easily uncover multipath from real GPS data than the conventional correlation. In this preliminary study, we performed coarse search of three satellites, namely, SVN2, 8 and 28. The despreading integration is 1 ms. The code delay search step is one sampling interval $\Delta t = 1/f_s$ with f_s = 17.357737 MHz, which is about 0.05894 chips, a rather fine value as the correlator spacing. The frequency search step is 500 Hz. In the acquisition mode without closed-loop tracking, a further reduction of the frequency search step may be used to minimize the effect of residual Doppler.

Since the code correlation is done over 1 ms, large variations are expected for sample behavior. Figures 5 and 6 show the correlation and normalized correlations for SVN2, respectively. The normalized correlation is another name for the generalized correlation, which we use interchangeably in this paper. The particular normalization in this example is the square-root normalized correlation as defined in Eq. (15). Figure 6 is clearer than Figure 5 to indicate the presence of a possible multipath in the late side (SVN2 is known to be subject to strong multipath).

At a first glance, the variations in the normalized correlation may be averaged out over time with more data. Without explicit tracking of the multipath components, only non-coherent integration is possible. Even with non-coherent integration, the sampling points of code delay may vary from block to block. Since the code and carrier replicas are tuned to catch up with the direct signal, their correlation with the multipath components actually penalizes it because of large frequency error losses.

It is interesting to note that the correlation power at the search Doppler bin plus one (red) is about the same as at the search Doppler bin minus one (blue) at the peak location (around 40) in Figure 5. This indicates that the search Doppler bin is quite close to the underlying signal frequency without a significant error. However, at the secondary peak (around 50), the correlation power at the search Doppler bin plus one (red) is higher than that at the search Doppler bin minus one (blue), indicating that the underlying signal frequency may be larger than the search Doppler bin. In other words, the frequency error of the multipath signal differs from that of the direct signal.

The observation is more evident with the normalized correlation in Figure 6. This suggests the possibility to implement a rake receiver with one tracking channel locked on to the direct signal and another on to the detected multipath signal. It appears that the normalized correlation in Figure 6 is clearly better than the conventional correlation in Figure 5 for the detection and eventually tracking of the multipath signal.

Figure 7 compares the conventional and normalized correlation functions together in the same plot at the search Doppler bin. The normalized correlation is more volatile than the conventional correlation in terms of sample variations and noise floor. As shown, the peak width is not significantly reduced because the filter's 3 dB bandwidth of 6 MHz is not much larger than 2 MHz of the signal. Nevertheless, the peak shape of the normalized correlation is indeed narrower than the conventional correlation.

Figures 8 and 9 show the comparison between the conventional correlation and normalized correlation for SVN8 and SVN28 at their search Doppler bin, respectively. It is clear from both figures that the normalized correlation has a narrower peak shape (by half) than the conventional correlation. Also note that the correlation peak values for the three satellites are between 3000 and 4000. This is consistent with what were shown for 1 ms integration in [Akos et al., 2004] (e.g., 3000 in Figure 17 and 4000 in Figure 23 of the paper).

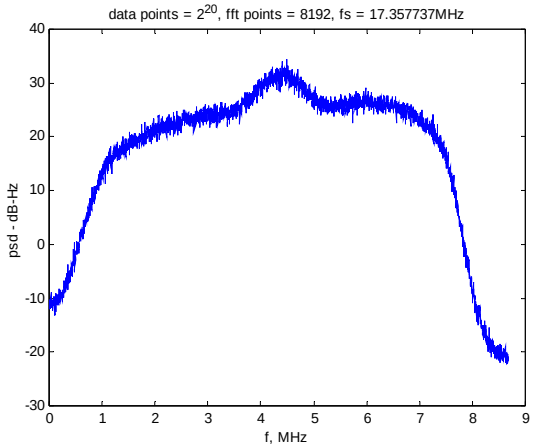

Figure 3 – Power Spectrum Density in dB

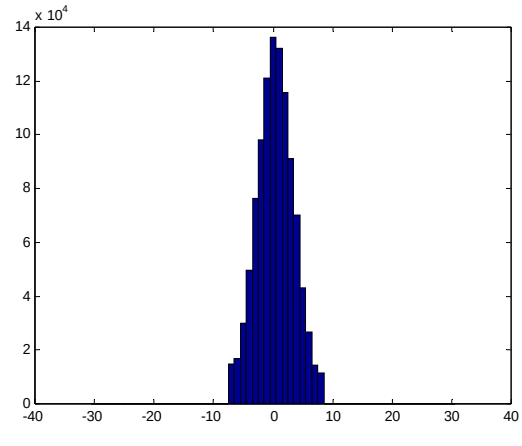

Figure 4 – Histogram for the First 10^{20} Data Points

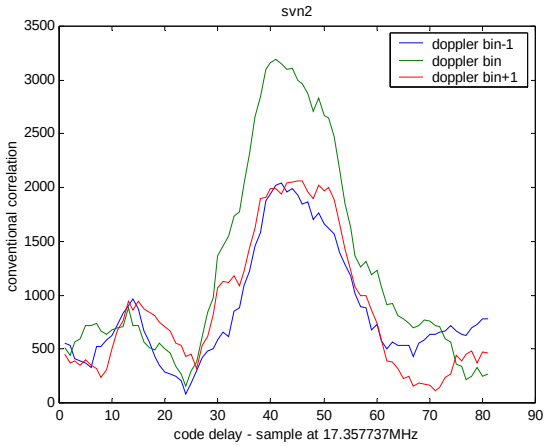

Figure 5 – Conventional Correlation Function at Three Doppler Values (SVN2)

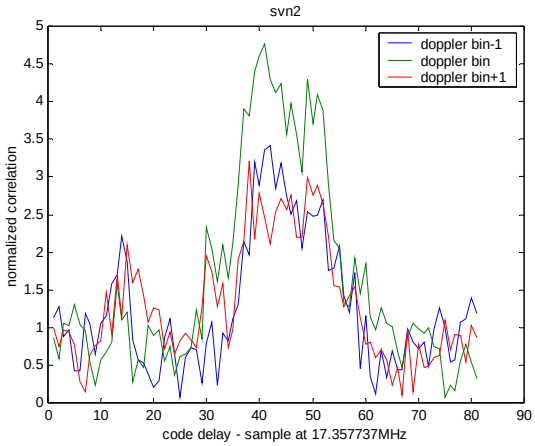

Figure 6 – Normalized Correlation at Three Doppler Values (SVN2)

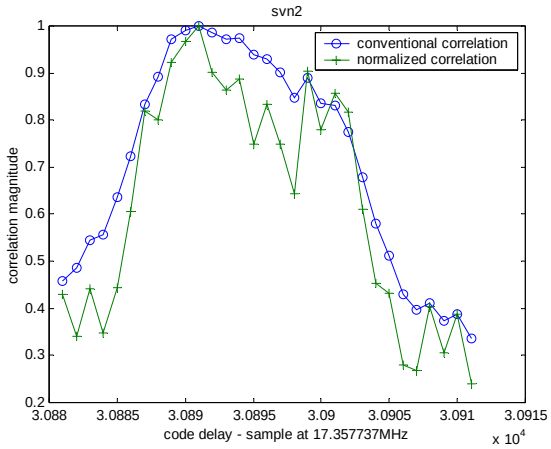

Figure 7 – Conventional vs. Normalized Correlation (SVN2)

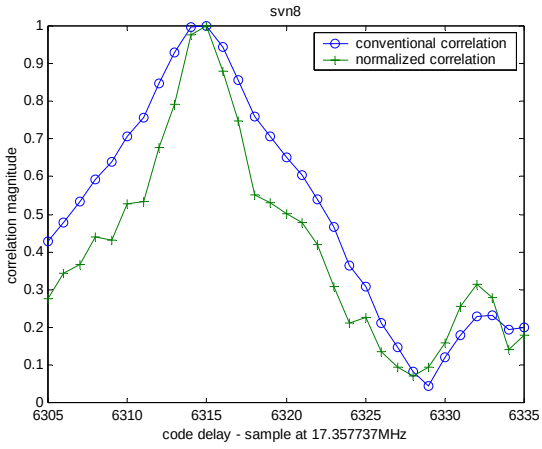

Figure 8 – Conventional vs. Normalized Correlation (SVN8)

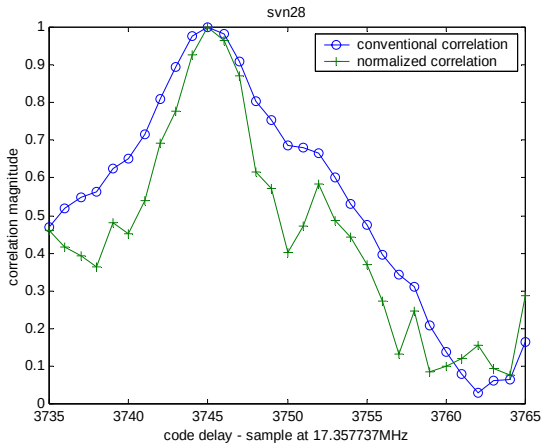

Figure 9 – Conventional vs. Normalized Correlation (SVN28)

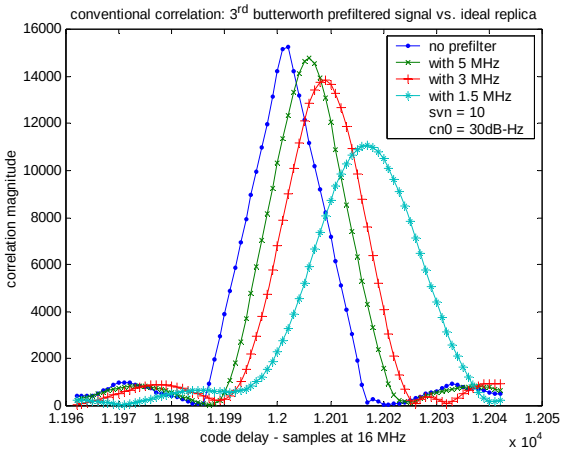

Figure 10 – Bandwidth on Conventional Correlation with Ideal Replica

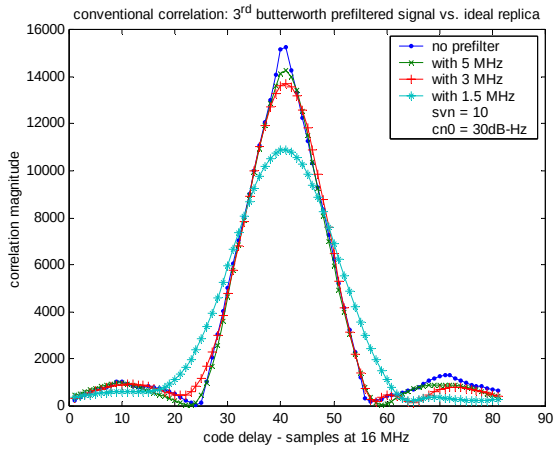

Figure 11 – Bandwidth on Conventional Correlation with Ideal Replica (Aligned)

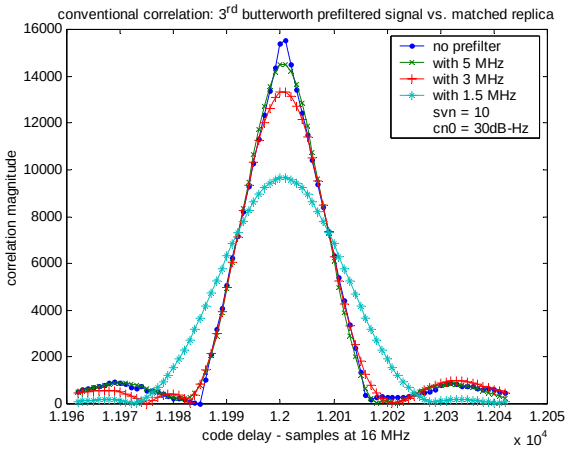

Figure 12 – Bandwidth on Conventional Correlation with Matched Replica (Aligned)

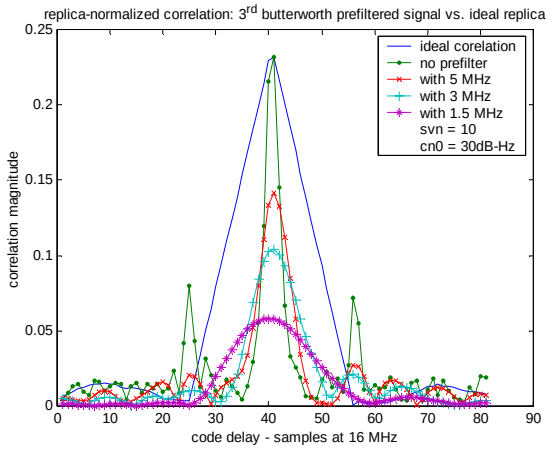

Figure 13 – Bandwidth on Replica-Normalized Correlation (Impulse Response, Ideal Replica, Aligned)

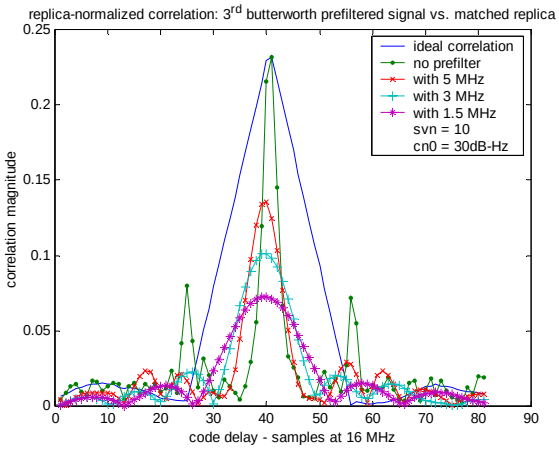

Figure 14 – Bandwidth on Replica-Normalized Correlation (Impulse Response, Matched Replica)

EFFECTS OF SIGNAL/RECEIVER BANDWIDTH

As shown in Figure 6, the normalized correlation appears to be a better indicator than the conventional correlation to reveal the presence of multipath because the green curve can tell the two peaks apart more clearly than the blue curve. However, the sharpness of a peak is affected by the effective bandwidth of the signal as it is limited by the modulating code, the transmitter, and the receiver as well. In addition, an ideal replica is used rather than the true frequency response of the transmitter-propagation-receiver's shaping filter. To assess these two aspects, we conducted the following simulations with the results analyzed below.

In the simulation, the initial carrier phase is drawn uniformly from 0 to 2π. A residual Doppler of 100 Hz is used. A complex Gaussian noise of unity variance is added. The signal amplitude is adjusted to simulate the desired C/N_0 level with $T_i = 0.001$ s according to:

$$A = (T_i 10^{\frac{C/N_0}{10}})^{\frac{1}{2}} \tag{16}$$

The ms boundary in the simulated signal is set between two sample points (0.45). The incoming signal is passed through a 3rd Butterworth lowpass filter with cutoff frequency selected for different bandwidth. The signal is sampled at 16 MHz.

Bandwidth Effect on Conventional Correlation ($\alpha = 0$)

The ideal replica code is used to correlate with the same incoming signal passing through four prefilters: no prefiltering, a prefilter with a cutoff frequency at 5 MHz, a prefilter with a cutoff frequency at 3 MHz, and a prefilter with a cutoff frequency at 1.5 MHz. The correlation is given in Eq. (11). The results are shown in Figure 9. To facilitate the comparison, the three curves are adjusted to align up in Figure 10.

The bandwidth has 4 effects: (1) round up the correlation at the peak, (2) lower the amplitude, (3) enlarge the base width, and (4) shift the peak due to group delay. The first three effects can be seen more clearly in Figure 10.

When the replica code is pre-filtered in exactly the same way as the incoming signal, the results are shown in Figure 11. Comparing Figure 11 with Figure 10 shows that, except for the amplitude and code shift, there is no much difference between the two in terms of the peak shape. This means it is acceptable to use the ideal code as the replica as far as the peak shape is concerned when conducting the conventional correlation.

Bandwidth Effect on Replica-Normalized Correlation ($\alpha = 1$)

When the correlation spectrum is normalized by the squared magnitude spectrum of the ideal code replica, it produces the impulse response of the satellite signal channel as defined in Eq. (12). Individual excision is applied to remove spurious spikes near multiples of the code chipping rate [Yang and Miller, 2005]. Figure 12 shows the impulse responses for signals with different bandwidths. Both the height and width of the peak are affected by the signal bandwidth. The curves were manually shifted in time for easy comparison.

When the correlation spectrum is normalized by the squared spectrum of the matched code replica, it still produces the impulse response of the satellite signal channel. But there was no need to align the normalized correlation functions for the matched replicas as shown in Figure 13 whereas the curves in Figure 12 have been shifted in time manually in order to display them together. The peaks in Figure 13 are only slightly different from (higher and narrower than) those in Figure 12 due to the matched filtering of replica. By consequence, the improvement if any may not warrant the use of a matched replica because of the amount of computation as far as the peak shape is concerned.

It can be seen from both Figures 12 and 13 that the replica normalized correlation (i.e., the impulse response) for the case where there is no prefiltering (not for the cases with prefiltering) exhibit sidelobes at $\pm T_c$ off the main peak. This can be understood as follows. Assume that the signal spectrum $S_0(f)$ subject to a delay D in additive noise, together with the replica, is given by:

$$S(f) = Ae^{-j2\pi fD}S_0(f) + N(f) \tag{17a}$$
$$R(f) = S_0(f) \tag{17b}$$

The corresponding impulse response is:

$$C(f) = \frac{S(f)}{R(f)} = \frac{[Ae^{-j2\pi fD}S_0(f) + N(f)]S_0^*(f)}{S_0(f)S_0^*(f)} = Ae^{-j2\pi fD} + \frac{N(f)}{S_0(f)} \tag{18}$$

When there is no noise, $N(f) = 0$, $C(f) = Ae^{-i2\pi fD}$. Theoretically, this C(f) is of constant magnitude and produces at D a single peak of a sinc-function with its nulls at $\pm T_s$. However, due to the discrete sampling nature of the underlying spectrum, S(f) and R(f) differ more than a complex exponential. In reality, the normalized spectrum is as shown in Figure 14 where the constant amplitude still holds for low frequencies but spikes show up at higher frequencies particularly around multiples of the chipping rate (which are amplified by the inverse of the signal spectrum which reaches nulls at the multiplicity of f_c).

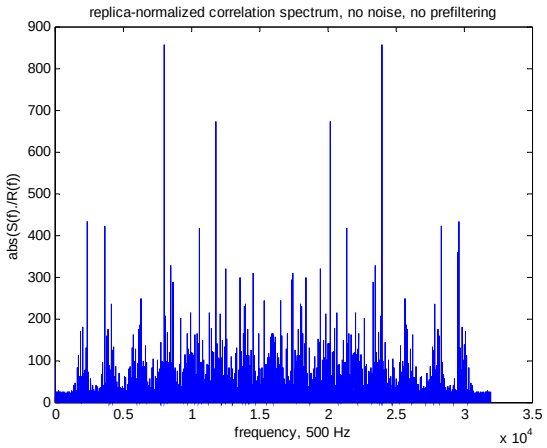

Figure 15 – Correlation Spectrum with Spikes at Chipping Rates

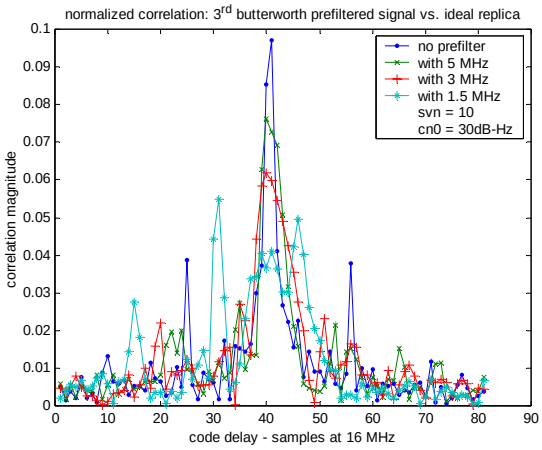

Figure 16 – Bandwidth on Normalized Correlation (Phase-Only, Ideal Replica, Aligned)

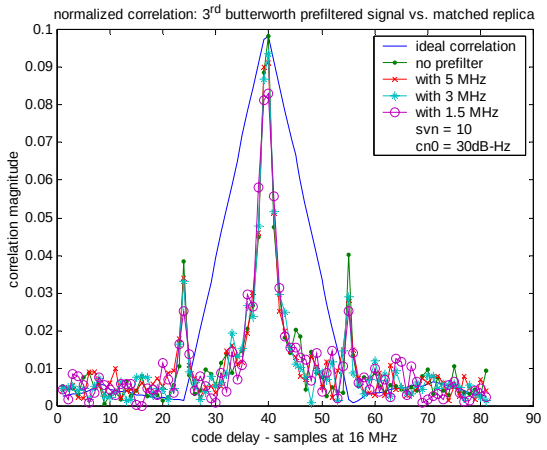

Figure 17 – Bandwidth on Normalized Correlation (Phase-Only, Matched Replica, Aligned)

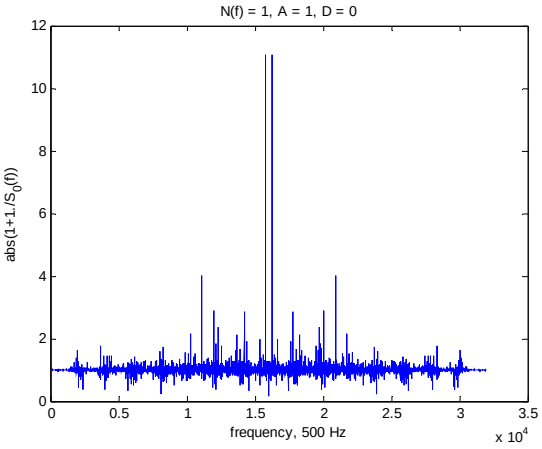

Figure 18 – Bandwidth on Normalized Correlation (Phase-Only, Matched Replica, Aligned)

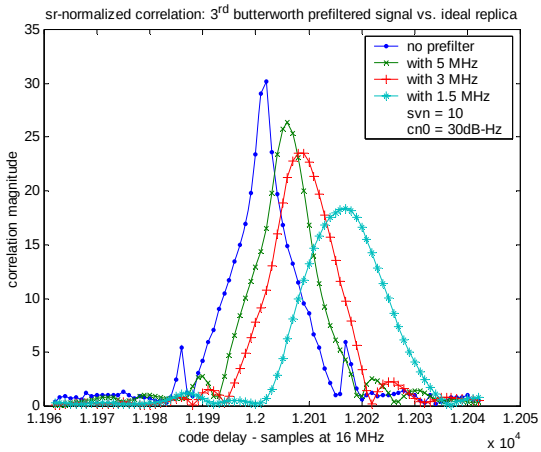

Figure 19 – Bandwidth on Square-Root Normalized Correlation (Ideal Replica)

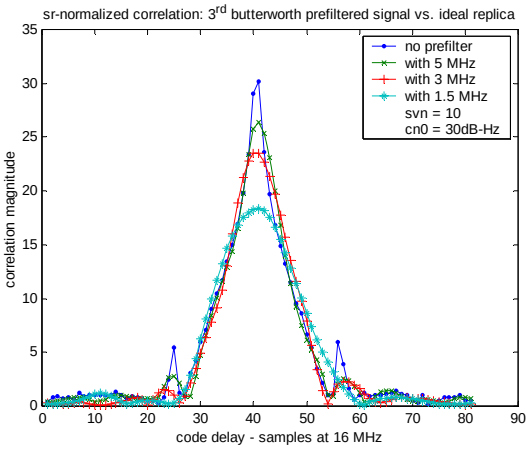

Figure 20 – Bandwidth on Square-Root Normalized Correlation (Ideal Replica, Aligned)

When converting the normalized spectrum Eq. (18) from the frequency domain back to the time domain, the normalized spectrum will be multiplied by the kernel function as:

$$\exp\{j2\pi f(D \pm nT_c)\} = \exp\{j2\pi fD\}\exp\{\pm j2\pi fnT_c\} \quad (19)$$

where T_c is the chip interval and n is the integer representing multiplicity of chip intervals.

The first term on the right hand side of Eq. (19) will cancel out with the numerator of the first term of Eq. (18). This leaves $e^{\pm i2\pi fnTc}$, which has a periodicity of T_c. The spikes, at multiples of the chipping rate as shown in Figure 14, contribute to the building up of sidelobes at $D\pm T_c$. Also evident from the figures, the sidelobes do not appear for the cases with prefiltering, which taper off the harmonic contributions rather rapidly.

Before taking the inverse Fourier transform, individual excision is applied to remove spurious spikes near multiples of the code chipping rate from the spectrum. With such spectrum filtering, the noise floor is lowered and the sidelobes (for the no prefilter case) are smaller but the main peak is widened from two samples per peak to about four samples per peak in Figures 12 and 13.

Assume that the signal passes through a filter H(f). The received signal and its matched replica can be written as:

$$S(f) = [Ae^{-j2\pi fD}S_0(f) + N(f)]H(f) \quad (20a)$$
$$R(f) = H(f)S_0(f) \quad (20b)$$

where N(f) is the noise spectrum. The replica-normalized correlation is:

$$C(f) = \frac{S(f)}{R(f)} = \frac{[Ae^{-j2\pi fD}S_0(f) + N(f)]H(f)H^*(f)S_0^*(f)}{H(f)S_0(f)H^*(f)S_0^*(f)}$$
$$= Ae^{-j2\pi fD} + \frac{N(f)}{S_0(f)} \quad |f| \le f_{ef} \quad (21)$$

where f_{eff} is the effective bandwidth of the signal and transmitter-receiver combined.

Eq. (21) looks the exactly the same as Eq. (18). Beyond the effective bandwidth, the spectrum normalization becomes "0/0 = 1" and it does not contain any useful information. This indicates that the height and width of the generalized correlation peaks is commensurate with the effective bandwidth f_{eff}. In contrast, the conventional correlation peaks are proportional to the code chip as shown in Figure 11. Also note that the excision threshold for spike components is another design parameter to trade for a particular implementation.

Bandwidth Effect on Normalized Correlation (α = 1)

When the correlation spectrum is normalized by itself, it produces the symmetric phase only matching as defined in Eq. (14) [Miller, Nguyen, and Yang, 2006]. With the ideal code replica, Figure 15 shows the symmetric phase-only matching for signals of different bandwidths. The peak width is affected by the signal bandwidth: the green and red curves vs. the blue curve. It is interesting to note that without the matched prefiltering (the blue curve), the response has two spikes at the conventional correlation nulls. For the narrowly filtered signal (the aqua curve), no global peak appears at the true timing but spikes around it.

With the matched replica, Figure 16 shows the symmetric phase-only matching, which all have about the same shape and are independent of the signal bandwidth. The width is slightly larger than two samples per side as predicted by the theory ($2T_s$).

Different from the replica-normalized correlation, sidelobes off the main peak by $\pm T_c$ are observed for the normalized correlation with and without prefiltering (except for no noise case). To understand this, express the normalized correlation spectrum for the matched and unmatched replicas, respectively, as:

$$C_{matched}(f) = \frac{S(f)R^*(f)}{|S(f)R^*(f)|} = \frac{[Ae^{-j2\pi fD}S_0(f) + N(f)]H(f)H^*(f)S_0^*(f)}{|[Ae^{-j2\pi fD}S_0(f) + N(f)]H(f)H^*(f)S_0^*(f)|}$$
$$= e^{-j2\pi fD}\frac{1 + \frac{N(f)}{Ae^{-j2\pi fD}S_0(f)}}{|1 + \frac{N(f)}{Ae^{-j2\pi fD}S_0(f)}|} \quad (22a)$$

$$C_{unmatched}(f) = e^{-j2\pi fD}\frac{[1 + \frac{N(f)}{Ae^{-j2\pi fD}S_0(f)}]}{|[1 + \frac{N(f)}{Ae^{-j2\pi fD}S_0(f)}]|}e^{j\phi[H(f)]} = C_{matched}(f)e^{j\phi[H(f)]} \quad (22b)$$

where $\phi[H(f)]$ represents the angle of H(f).

The numerator of Eq. (22a) is plotted in Figure 17 with N(f) = 1 and A = 1.It shows an average value (spectral dc component) at 1 and spikes at multiples of the chipping rate. The latter explains the building of sidelobes at $D\pm T_c$ as shown in Figures 15 and 16.

It has been observed that for the cases with a matched replica there is a rather significant peak appears at the zero delay, which corresponds to a spectral average value as shown in Figure 17. This bias can be ignored or removed from the dc component of the inverse Fourier transform. With unmatched replicas, the dc component is scrambled by the extra phase term as shown in Eq. (22b) and there is therefore no peak at the zero delay.

In the matched replica case, although the filter H(f) does not show up in Eq. (22a) because of cancellation, S(f) and R(f) contains no information beyond the effective bandwidth, $|f| \le f_{eff}$. However, the magnitude of Eq. (22a) is always of unity. In the unmatched case, the magnitude of Eq. (22b) remains to be unity but there is an extra phase term related to the filter, which is cause of the differences between Figures 15 and 16. This suggests that for the normalized correlation, it is preferred to use the matched replica for better performance.

Bandwidth Effect on Square-Root Normalized Correlation (α = ½)

Figure 18 shows the square-root normalized correlations between the incoming signal of different bandwidths and the ideal replica as defined in Eq. (15). Figure 19 is the same as Figure 18 except that the four curves are manually shifted together for easy comparison.

Without prefiltering, sidelobes located at $D \pm T_c$ are observed for the square-root normalized correlation for similar reasons explained in Section 4.2 for the replica-normalized correlation (i.e., the impulse response) and in Section 4.3 for the normalized correlation (i.e., the symmetric phase-only matching).

The square-root normalized correlation has a peak shape similar to, but with a base width larger than, the replica-normalized correlation as shown in Figure 12. The square-root normalized correlation is affected by the signal bandwidth in four ways: (1) round up the correlation at the peak, (2) lower the amplitude, (3) enlarge the base width, and (4) shift the peak due to group delay.

Figure 20 shows the square-root normalized correlations between the incoming signal of different bandwidths and the bandwidth-matched filtered replica. The use of filtered replica did not bring any improvement in the correlation shape but rather catches up with the extra code shift due to group delay. No curve alignment was needed.

Figure 21 shows the four square-root normalized correlations as compared to the ideal conventional correlation. They all have smaller peak width than the conventional correlation although it becomes less advantageous as the bandwidth becomes smaller and smaller.

It is interesting to note that the square-root normalized correlation starts to sharpen its peak when closer to 1/3 of the code chip. It has lower noise floor than the replica-normalized correlation. Although it has a wider base, its peak becomes narrower than the replica-normalized correlation once within 1/3 of a code chip. The comparison of these three correlation functions are shown in Figure 22.

Additional simulation results for such aspects as code-independence and multipath performance of the generalized frequency-domain correlator can be found in [Miller, Nguyen, and Yang, 2006].

CONCLUSIONS

In this paper, the generalized frequency-domain correlator (GFDC) was introduced with its advantages analyzed for use in a software GPS receiver. Various implementation schemes of the GFDC were formulated. A set of GPS data recorded on a large aircraft were used to demonstrate the ability of the GFDC to uncover closely-spaced multipath signals more easily than the conventional correlators.

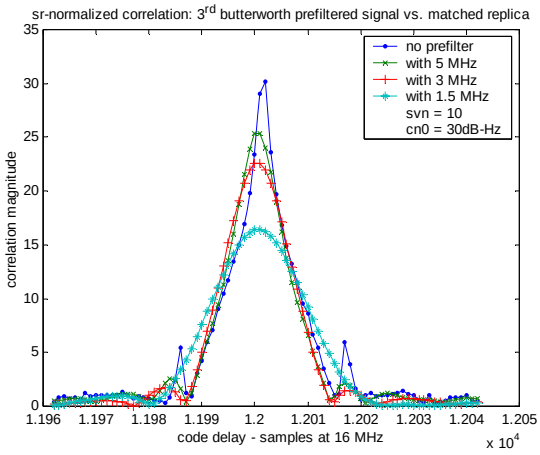

Figure 21 – Bandwidth on Square Root Normalized Correlation (Matched Replica)

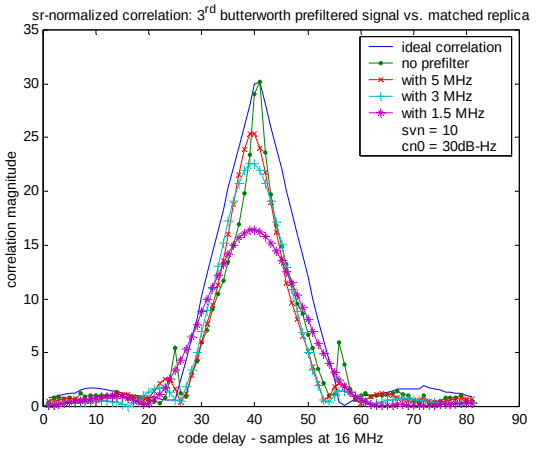

Figure 22 – Bandwidth on Square Root Normalized Correlation (Matched Replica) vs. Ideal Conventional Correlation

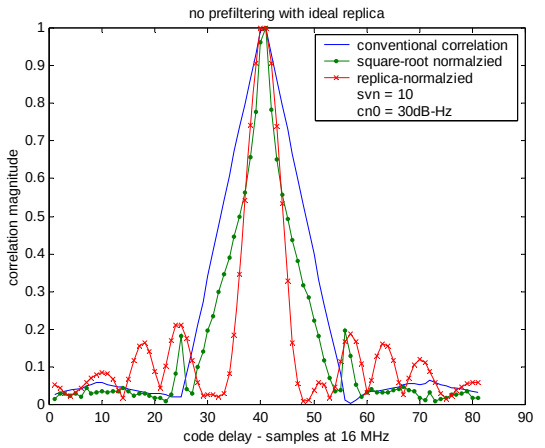

Figure 23 – Square-Root and Replica-Normalized Correlations vs. Conventional Correlation

In addition, the practical issue of limited bandwidth and its effects on both the conventional correlators and the GFDC were analyzed via simulation. It showed that any limit in signal bandwidth not only flattened the conventional correlation at the peak but also enlarged its base width beyond the nominal code chip duration. It is this enlargement of the base width that makes the conventional correlation vulnerable to multipath. In contrast, the base width of the normalized correlation peak was also affected by the bandwidth of signals. But it remained smaller than the conventional correlation (up to the inverse of the effective bandwidth). It is this advantage that enables the normalized correlation to have a better multipath performance and a more accurate timing estimation.

As shown in the paper, it was difficult to perform coherent integration for both the direct and multipath signals at the same time because of their difference in frequency. To extend the snapshot results presented in this paper to much longer periods, it is necessary to conduct separate tracking for the multipath signals at the same time as the direct signal in order to gain better assessment. The generalized frequency-domain correlator tuned to the direct signal, with its narrow peak base width, may also serve as the joint code and frequency error discriminator for the multipath signals. Efforts are under way to evaluate this idea for multipath capturing and analysis.

ACKNOWLEDGMENTS

Research supported in part under Contract No. FA8650-05-C-1828, which is gratefully acknowledged. Two U.S. patents are pending (2004 and 2005).

REFERENCES

D.M. Akos, J.P. Weiss, T. Murphy, and S. Pullen, "Airborne Multipath Investigation via a GPS Software Receiver," *Proc. of ION-GNSS'2004*, September 2004.

J.W. Betz, "Binary Offset Carrier Modulation for Radionavigation," *Navigation: The Journal of the Institute of Navigation*, 48(4), Winter 2001-2002.

Q.S. Chen, M. Defrise, and F. Deconick, "Symmetric Phase-Only Matched Filtering of Fourier-Mellin Transforms for Image Registration and Recognition," *IEEE Trans. Pattern Analysis and Machine Intelligence*, 16(12), Dec. 1994.

P. Fine and W. Wilson, "Tracking Algorithm for GPS Offset Carrier Signals," *ION-NTM'99*, January 1999.

J.C. Hassab and R.E. Boucher, "Optimum Estimation of Time Delay By A Generalized Correlator," *IEEE Trans. Acoust. Speech Signal Process.*, 27, 1979.

E.D. Kaplan (ed.), *Understanding GPS: Principles and Applications*, Artech House Publishers, Norwood, MA, 1996.

C.H. Knapp and G.C. Carter, "The Generalized Correlation Method for Estimation of Time Delay," *IEEE Trans. Acoust. Speech Signal Process.*, 24, 1976.

M. Miller, T. Nguyen, and C. Yang, "Symmetric Phase-Only Matched Filter (SPOMF) for Frequency-Domain Software GNSS Receivers," *Proc. of ION-AM/IEEE-PLANS*, April 2006.

P. Misra and P. Enge, *Global Positioning System, Signals, Measurements, and Performance*, Ganga-Jamuna Press, 2001.

A.V. Oppenheim and J.S. Lim, "The Importance of Phase in Signals," *Proceedings of the IEEE*, 69(5), May 1981.

B.W. Parkinson, and J.J. Spilker Jr. (eds.), *Global Positioning System: Theory and Applications*, AIAA, 1996.

J.B.Y. Tsui, *Fundamentals of Global Positioning System Receivers - A Software Approach*, John Wiley & Sons, Inc., 2000.

M.P. Wernet, "Symmetric Phase Only Filtering: A New Paradigm for DPIV Data Processing," *Measurement Science and Technology*, 16, 2005.

C. Yang, "Frequency-Domain GPS Baseband Processor Design and Initial Test Results," *Proc. of ION-GPS'01*, Sept. 2001a.

C. Yang, "FFT Acquisition of Periodic, Aperiodic, Punctual, and Overlaid Codes in GPS," *Proc. of ION-GPS'01*, Sept. 2001b.

C. Yang, "Tracking of GPS Code Phase and Carrier Frequency in the Frequency Domain," *Proc. of ION-GPS/GNSS'03*, Sept. 2003.

C. Yang, "GPS Signal Tracking with Kalman Filter Based on Joint Code Delay and Carrier Phase and Frequency Error Discriminator," *ION-AM'04*, June 2004.

C. Yang, "Frequency-Domain GPS Receiver for Modernization GPS Signals via Full-Band Multi-Code Processing," *ION-GNSS'05*, September 2005.

C. Yang and M. Miller, "Novel GNSS Receiver Design Based on Satellite Signal Channel Transfer Function/Impulse Response," *ION-GNSS'05*, September 2005.

C. Yang, M. Miller, and T. Nguyen, "Block-Repetitive Iterated Processing for Software GPS Receiver: Dichotomized Search for Correlation Peak," To Be Submitted to *ION-GNSS'06*, September 2006.

C. Yang and A. Porter, "Multipath Desensitized Delay Estimation with GPS Signal Channel Transfer Function Filtering," *ION-AM'05*, June 2005.

C. Yang, J. Vasquez, and J. Chaffee, "Frequency-Domain Doppler Search and Jam-Suppression for Fast Direct P(Y)-Code Acquisition," *Proc. of ION-GPS'99*, Sept. 1999.